

Efficient Computation of Spectral Moments for Determination of Random Response Statistics

Karl A. Sweitzer

Eastman Kodak Company, Rochester, NY USA

& Institute of Sound and Vibration Research, University of Southampton, UK

email: karl.sweitzer@kodak.com

Neil W. M. Bishop

Random Loading and Design Ltd, Surrey UK

Victor L. Genberg

Sigmadyne Inc., Rochester, NY USA

Abstract

This paper will first review the use of temporal spectral moments, and then propose an efficient running sum technique to determine the spectral moments frequency by frequency. Combining this summation process with modal superposition techniques allow a significant reduction in input and output file sizes and computational time.

The proposed technique uses finite element analysis (FEA) to generate modal vectors that are postprocessed using mode superposition techniques to calculate the power spectral density (PSD) moments, eliminating the need to form PSD response functions. This requires storage of only the modal response and force vectors and the running sum of the PSD moments. Once the moments of the PSD are determined, the random response statistic calculations are a straightforward problem. Two example problems are given: a simple cantilever beam and a detailed optical telescope. These examples show how different problems can be solved using the proposed technique.

1 Introduction

A review of spectral moment and derivative process calculation is given below. For a full treatment of the subject, see [1-4].

Spectral moments are calculated from the one-sided PSD $G(f)$ (in units of Hertz) or the two-sided PSD $S(\omega)$ (in units of radians) using

$$m_n = \int_0^{\infty} f^n G(f) df \quad (1)$$

$$\mu_n = \int_{-\infty}^{\infty} \omega^n S(\omega) d\omega = m_n (2\pi)^n \quad (2)$$

m_n is usually the version used because it results in more refined equations for the numbers of zero crossings and peaks.

1.1 PSD and autocorrelation functions

In order to understand what “moments” are all about, we need to consider some definitions. The autocorrelation function that defines how a signal is correlated with itself, with a time separation τ is

$$R_{xx}(\tau) = \int_{-\infty}^{\infty} x(t) x(t + \tau) dt = E[x(t) x(t + \tau)] \quad (3)$$

The autocorrelation and PSD functions are related by the Fourier transform pair

$$S_{xx}(\omega) = \frac{1}{2\pi} \int_{-\infty}^{\infty} R_{xx}(\tau) e^{-j\omega\tau} d\tau \quad (4)$$

$$R_{xx}(\tau) = \int_{-\infty}^{\infty} S_{xx}(\omega) e^{j\omega\tau} d\omega \quad (5)$$

As S_{xx} is a real even-valued function

$$R_{xx}(\tau) = \int_{-\infty}^{\infty} S_{xx}(\omega) \cos \omega\tau d\omega \quad (6)$$

By differentiating $R_{xx}(\tau)$ several times (with respect to τ), we can obtain the following results

$$R'_{xx}(\tau) = -R_{\dot{x}\dot{x}}(\tau) = -\int_{-\infty}^{\infty} \omega S_{xx}(f) \sin \omega\tau df \quad (7)$$

$$R''_{xx}(\tau) = -R_{\ddot{x}\ddot{x}}(\tau) = -\int_{-\infty}^{\infty} \omega^2 S_{xx}(f) \cos \omega\tau df \quad (8)$$

$$R'''_{xx}(\tau) = -R_{\dot{x}\ddot{x}}(\tau) = \int_{-\infty}^{\infty} \omega^3 S_{xx}(f) \sin \omega\tau df \quad (9)$$

$$R''''_{xx}(\tau) = R_{\ddot{x}\dot{x}}(\tau) = \int_{-\infty}^{\infty} \omega^4 S_{xx}(f) \cos \omega\tau df \quad (10)$$

The moments, therefore, define how each of the processes x , \dot{x} , \ddot{x} , etc. are related to the other processes when $\tau = 0$, i.e.,

$$\mu_n = \frac{d^n}{d\tau^n} R_{xx}(0) = \frac{d^n}{dt^n} R_{xx}(0) = \int_{-\infty}^{\infty} \omega^n S_{xx}(f) df \quad (11)$$

or in terms of the one-sided PSD $G(f)$

$$\mu_n = \int_0^{\infty} (2\pi f)^n 2S_{xx}(f) df = (2\pi)^n \int_0^{\infty} f^n G_{xx}(f) df = m_n (2\pi)^n; \quad m_n = \int_0^{\infty} f^n G_{xx}(f) df \quad (12)$$

It is important to note that μ_1 and μ_3 are zero, but m_1 and m_3 are not. Remember that μ_n is produced by integrating from $-\infty$ and $+\infty$, and m_n is produced by integrating from 0 to $+\infty$. Typically, we calculate m_0 , m_1 , m_2 and m_4 .

1.2 Application of spectral moments

The most common spectral moment is μ_0 , which determines the variance of a PSD

$$\mu_0 = \sigma_x^2 = \int_{-\infty}^{\infty} S_{xx}(\omega) d\omega = 2 \int_0^{\infty} S_{xx}(\omega) d\omega = \int_0^{\infty} G(f) df = m_0 \quad (13)$$

Note that, in this case, μ_0 and m_0 are equal. The root mean square (rms) value of the zero mean process is given by $\sqrt{m_0}$. Several examples of rms response calculations are given later in this paper.

A more complicated example of the use of these moments considers the number of zero crossings in a stationary random and Gaussian (normal) process. Consider the two-dimensional probability function $p(\alpha, \beta)$ of x and \dot{x}

$$p(\alpha, \beta) \Delta\alpha \Delta\beta \approx \text{Prob}[\alpha \leq x(t) \leq \alpha + \Delta\alpha \quad \text{and} \quad \beta \leq \dot{x}(t) \leq \beta + \Delta\beta] \quad (14)$$

This probability represents the fraction of time that x is between α and $\alpha + \Delta\alpha$, when the velocity \dot{x} is between β and $\beta + \Delta\beta$. If we define the time to cross one interval as Δt , we get

$$\Delta t = \frac{\Delta\alpha}{|\beta|} \quad (15)$$

From which we can obtain the expected total number of positive crossings of level α by dividing (12) by Δt and integrating over all positive values of β .

$$\frac{p(\alpha, \beta) \Delta\alpha \Delta\beta}{\Delta t} \approx |\beta| p(\alpha, \beta) \Delta\beta \quad (16)$$

As $\Delta\beta \rightarrow 0$, the total expected number of passages per unit time through $x(t) = \alpha$ for all possible values of β is given by

$$E[\alpha] = \int_0^{\infty} |\beta| p(\alpha, \beta) d\beta \quad (17)$$

By setting $\alpha = 0$, we get the required number of zero crossings per unit time

$$E[0] = \int_0^{\infty} |\beta| p(0, \beta) d\beta \quad (18)$$

The two-dimensional normal density function of x and \dot{x} is given by

$$p(\alpha, \beta) = (2\pi)^{-1} |A|^{-0.5} e^{\left[\frac{-1}{2|A|} (A_{11}\alpha^2 + 2A_{12}\alpha\beta + A_{22}\beta^2) \right]} \quad (19)$$

Where

$$A = \begin{bmatrix} a_{11} & a_{12} \\ a_{21} & a_{22} \end{bmatrix} \quad (20)$$

And

$$a_{ij} = E[x_i x_j] = a_{ji} \quad (21)$$

The a_{ij} terms are the covariances or second moments of x_i and x_j . The a_{ii} terms are the variances of x_i and x_j . $|A|$ is the determinant of A and A_{ij} is the cofactor of a_{ij} .

With a little effort, we get

$$\begin{aligned} a_{11} &= R(0) = \mu_0 \\ a_{12} &= a_{21} = \mu_1 = 0 \\ a_{22} &= \mu_2 \end{aligned} \quad (22)$$

Therefore,

$$A = \begin{bmatrix} \mu_0 & 0 \\ 0 & \mu_2 \end{bmatrix} \quad (23)$$

From which we get

$$E[\alpha] = \frac{1}{2\pi} \left[\frac{\mu_2}{\mu_0} \right]^{1/2} e^{-\frac{\alpha^2}{2\mu_0}} \quad (24)$$

If we set $\alpha = 0$, we get the important result

$$E[0] = \left[\frac{m_2}{m_0} \right]^{1/2} \quad (25)$$

In a similar way, we can derive results for the number of peaks, P , and points of inflection, PI , per unit time

$$E[P] = \left[\frac{m_4}{m_2} \right]^{1/2} \quad (26)$$

$$E[PI] = \left[\frac{m_6}{m_4} \right]^{1/2} \quad (27)$$

1.3 Response statistics based on spectral moments

Spectral moments have an important part to play in the determination of several wideband (and in the limit, narrowband) response probability density functions (PDFs). The following sections define a general peak PDF for use on a wide range of problems and a Rainflow range PDF for use with random fatigue damage calculations.

1.3.1 General peak probability density function

A general peak PDF [1] for the standardized variable v (zero mean and unit variance) is expressed as (see [3] for a slightly different development)

$$p(v) = \left(\frac{k_1}{\sqrt{2\pi}} \right) \exp\left(-\frac{v^2}{2k_1^2}\right) + \varpi v \exp\left(-\frac{v^2}{2}\right) \left[1 - Q_n\left(\frac{v}{k_2}\right) \right] \quad (28)$$

where the dimensionless ratio of expected rate of zero crossings $E[0]$ to peaks $E[P]$ is

$$\frac{E[0]}{E[P]} = \left[\frac{m_2}{\sqrt{m_0 m_4}} \right] = \varpi \quad (29)$$

The other terms in (28) are

$$\begin{aligned} k_1^2 &= 1 - \varpi^2 & k_2 &= k_1 / \varpi \\ Q_n\left(\frac{v}{k_2}\right) &= \frac{1}{\sqrt{2\pi}} \int_{v/k_2}^{\infty} \exp\left(-\frac{u^2}{2}\right) du = \frac{1}{2} \operatorname{erfc}\left(\frac{v}{\sqrt{2} k_2}\right) \end{aligned} \quad (30)$$

where **erfc** is the complimentary error function. For a narrowband response problem $\varpi \rightarrow 1$ and (28) simplifies to the Rayleigh PDF:

$$p(v) = v \exp(-v^2/2) \quad (31)$$

Similarly, as the problem becomes completely wideband, $\varpi \rightarrow 0$ and (28) simplifies to the Gaussian PDF:

$$p(v) = (1/\sqrt{2\pi}) \exp(-v^2/2) \quad (32)$$

Peak displacement examples using (28) will be presented later in the paper.

1.3.2 Spectral moments and fatigue

Important fatigue parameters can be computed using spectral moments of a stress response PSD. Early narrowband fatigue life theories [2-6] assumed that damage estimates D_n could be based on the Rayleigh peak PDF $p(a)$ (31) and the rate of zero crossings $E[0]$ (25)

$$E[D_n] = E[0] \frac{T}{c} \int_0^\infty a^\beta p(a) da = E[0] \frac{T}{c} (\sqrt{2}\sigma)^\beta \Gamma\left(1 + \frac{\beta}{2}\right) \quad (33)$$

where T is the period of the time history, a is the stress amplitude, σ is the rms stress (13) and Γ is the Gamma function. The material properties β and c are determined empirically from sinusoidal ‘‘S-N’’ fatigue tests. More recent fatigue damage theories [7-10] are based on the wideband stress Rainflow range cycle density $p(\Delta)$ and the rate of peaks $E[P]$ (26)

$$E[D_w] = E[P] \frac{T}{k} \int_0^\infty \Delta^\beta p(\Delta) d\Delta \quad (34)$$

where the material property $k=2^\beta c$. One approximation for $p(\Delta)$ is given by Dirlik’s expression [7]

$$p(\Delta)_D = \frac{1}{2\sqrt{m_0}} \left(\frac{d_1}{q} \exp\left(\frac{-\alpha}{q}\right) + \frac{d_2 \alpha}{r^2} \exp\left(\frac{-\alpha^2}{2r^2}\right) + d_3 \alpha \exp\left(\frac{-\alpha^2}{2}\right) \right) \quad (35)$$

where the variable Δ is a range value (2X amplitude). Note that, like (28), Dirlik’s expression assumes zero mean value, but unlike (28), (35) normalizes the range Δ to a unit variance α within the expression. The terms in (35) are functions of the spectral moments:

$$\alpha = \frac{\Delta}{2\sqrt{m_0}} \quad \varpi = \frac{m_2}{\sqrt{m_0 m_4}} \quad \eta = \frac{m_1}{m_0} \sqrt{\frac{m_2}{m_4}} \quad (36)$$

The other terms in (35) are:

$$d_1 = \frac{2(\eta - \varpi^2)}{1 + \varpi^2} \quad r = \frac{\varpi - \eta - d_1^2}{1 - \varpi - d_1 + d_1^2} \quad d_2 = \frac{(1 - \varpi - d_1 + d_1^2)}{1 - r} \quad (37)$$

$$d_3 = 1 - d_1 - d_2 \quad q = \frac{1.25}{d_1} [\varpi - d_3 - (d_2 r)]$$

Traditionally, the moments of stress PSD are found as a two-step process. First, a forced response FEA analysis is run with a unit vibration or acoustic load. The output of this analysis is a set of complex stress transfer functions for the elements of interest.

The second step is performed by a fatigue analysis post-processing program. This program reads the complex stress transfer functions into memory, multiplies by the PSD of the input load, finds the principal

stress magnitude, and integrates them over the frequency range of interest to find the spectral moments. The main problem is the large storage requirements for the stress transfer functions at the many discrete frequencies of interest.

1.4 Transfer functions based on modal superposition

Transfer functions of response parameters for input loads are easily determined by the modal superposition method. The following sections develop the theory for standard displacement transfer functions as well as other useful transfer functions based on linear transformations.

1.4.1 Modal displacement superposition

Probably the most well-known modal superposition method is based on modal displacements. Standard analysis programs (e.g., FEA) produce eigenvalues λ and modal displacement vectors ϕ for ν modes of interest. The modal displacement basis vector ϕ is defined here as the mass-normalized eigenvector such that

$$\phi_i^t M \phi_i = 1 \quad (38)$$

One other analysis result, the modal force vector γ , is required from the analysis program

$$\gamma_i = \phi_i^t F \quad (39)$$

where it is convenient for F to be a unit load with units consistent with the dynamic load. The unit load is used by the proposed spectral postprocessing technique to generate a complex transfer function H between component responses and the applied dynamic load by mode superposition [11]

$$H_{xF}(s) = \sum_{i=1}^{\nu} \frac{\gamma_i \phi_i}{(s^2 + 2\delta_i \lambda_i s + \lambda_i^2)} \quad (40)$$

where δ_i are modal damping scalars, and s is the complex Laplace operator. Equation (40) represents the proportionally damped linear superposition form of the transfer function. Other forms of damping (e.g., hysteretic or viscous damping) and eigenvectors (i.e., complex eigenvectors) can be analyzed with similar complex transfer function notation.

1.4.2 Modal stress superposition

Modal stress superposition is a logical extension of modal displacement superposition [12]. As before, FEA analysis programs are used to produce eigenvalues λ , modal force scalars γ and to determine modal stress vectors ξ for ν modes. The modal stress vector is defined here as a vector of element stresses for an imposed mass-normalized eigenvector displacement. It is determined, given the stress displacement relationship

$$\sigma = Y\varepsilon, \varepsilon = Bx, \sigma = YBx \quad (41)$$

where σ is the element stress vector (a second-order symmetric tensor), Y is the material matrix, B is the strain displacement matrix and ε is the strain vector for a displacement vector x . Substituting a mass-normalized eigenvector ϕ_i for the displacement vector x gives the modal stress vector

$$\xi_i = YB\phi_i \quad (42)$$

The modal stress vectors ξ contain component stresses for each element. The stress transfer function is

$$H_{\sigma F}(s) = \sum_{i=1}^{\nu} \frac{\gamma_i \xi_i}{(s^2 + 2\delta_i \lambda_i s + \lambda_i^2)} \quad (43)$$

After superposition, the complex element component stresses are used to calculate element principal, octahedral, or von Mises stresses and directions. The change in the principal stress directions, as a function of frequency, gives a keen insight into the geometric state of stress in the element (i.e., is it axial or multi-axial).

1.4.3 Modal optomechanical response superposition

A more specialized use of mode superposition has been developed for optical systems with flexible reflective surfaces [13]. This technique is based on a set of optical basis functions called Zernike coefficients [14-15] that describe the rigid body motions and deformations of the reflective surfaces. Displacement vectors x are used in a surface fitting program [16] to determine the t Zernike coefficients D_i for each reflective surface. These surface Zernike terms are combined with an optical system sensitivity matrix S to determine the overall optical system performance in terms of wavefront error and image motion. The overall system Zernike terms for a displacement vector x is another linear transformation:

$$Z = SDx \quad (44)$$

For the mode superposition implementation, an FEA program is used to generate modal parameters (eigenvalues λ , modal force scalar γ , and modal displacement vectors ϕ) for ν eigenvalues of interest. The modal displacement vectors ϕ are used to determine the t Zernike coefficients D_{ii} for mode i for each reflective surface.

$$\zeta_i = SD\phi_i \quad (45)$$

where ζ are the modal Zernike coefficients for the combined system of flexible optics. The subsequent optical response transfer function is:

$$H_{ZF}(s) = \sum_{i=1}^{\nu} \frac{\gamma_i \zeta_i}{(s^2 + 2\delta_i \lambda_i s + \lambda_i^2)} \quad (46)$$

These optical response transformations [13] and the proposed running sum technique have been implemented as a modal post processing function in SigMax [17].

1.5 Response PSD at a frequency

Having developed transfer functions between responses and the applied load, the response PSD G for a single input load PSD W can be found at any frequency f_k :

$$G(f_k) = |H(f_k)|^2 W(f_k) \quad (47)$$

The point of this development is that response PSD $G(f_k)$ can be calculated at any frequency based on a compact set of transfer functions from (40), (43) or (46).

2 Proposed technique

To reduce the amount of storage, an efficient technique for calculating the spectral moments for linear systems has been developed. The proposed technique uses FEA as an analysis engine to find modal parameters. These modal parameters are superimposed in a running sum technique to find the spectral moments.

2.1 Running sum of moments

The key to the proposed technique is to calculate the spectral moments using a running sum. A discrete-frequency rectangular-integration approximation to (1) is proposed

$$m_n = \sum_{i=0}^l f_i^n G(f_i) \Delta f_i = \sum_{i=0}^l m_n \quad (48)$$

where Δf is the discrete frequency spacing. The response PSD $G(f)$ is from (47). The summation can be thought of as a loop over frequency where, at any calculation frequency f_k , the sum is made up of the previous sum (or running sum), the current calculation and the future sums

$$m_n = \sum_{i=0}^{k-1} m_n + f_k^n G(f_k) \Delta f_k + \sum_{j=k+1}^l m_n \quad (49)$$

For simplicity, let the running sum of spectral moments be

$$\Sigma m_n = \sum_{i=1}^{k-1} m_n \quad (50)$$

Using this technique, a minimum set of terms needs to be stored in memory to find the spectral moments. They are

$$\begin{aligned} \Sigma m_n; n = 0, 1, 2, 4 \\ \lambda_i, \delta_i, \gamma_i; i = 1, \nu \end{aligned} \quad (51)$$

the four spectral moment running sums Σm_n and the modal parameters for ν modes of interest. The modal response terms ϕ_i, ξ_i, ζ_i , from (38), (42) or (45) must also be stored or calculated, depending on what type of response is desired. No storage of discrete frequency data block results is required. Equations (48-50) can easily be extended to higher-order integration.

If desired, each response term may be output (e.g., for further XY plotting) at the same number of frequency lines as the running sums are computed, or at a reduced number of lines to conserve file size. Each mode's contribution to the net spectral moment can also be output, so major modal contributors can be identified.

2.2 Analysis flow charts for baseline and proposed methods

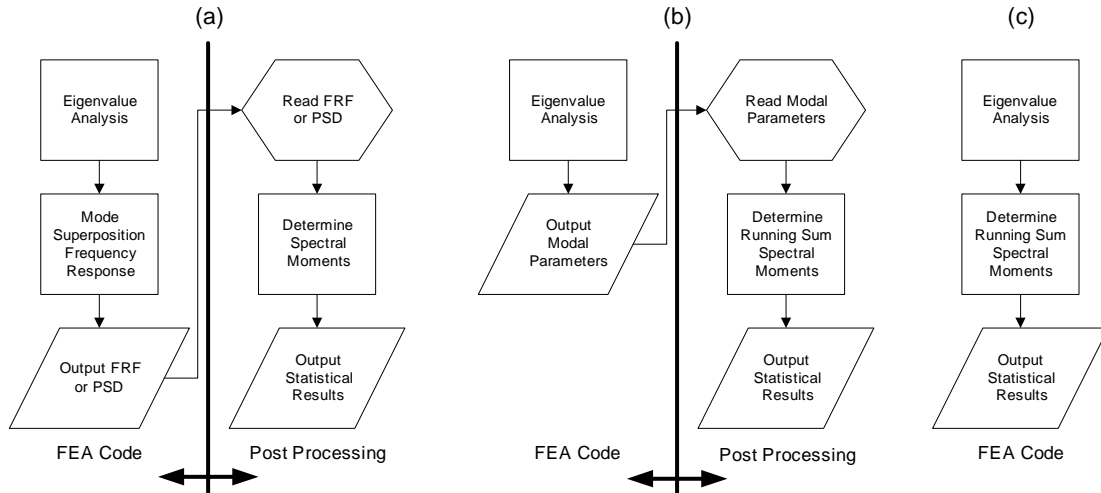


Figure 1: Flow charts for baseline (a) and proposed (b and c) running sum methods

The baseline method, Figure 1(a), starts with an eigenvalue solution (for ν modes) in an FEA program, followed by a solution to determine response transfer functions or response PSDs (for k DOF), over a range of l frequencies. These response functions are written to storage files (of size $k * l$) for transfer to another postprocessing program. Here, the response functions are integrated over the frequency range to determine spectral moments using (12).

The proposed method, Figure 1(b), starts with the same eigenvalue solution whose parameters (for ν modes at k DOF) are written to storage files (of size $k * \nu$). In this case, a postprocessing program calculates spectral moments using the running sums as described in section 2.1. Clearly, the proposed technique is more efficient when the number of required solution frequencies l is greater than the number of modes ν . The method shown in Figure 1(b) also can be extended to other linear transformations as discussed in section 1.4.3.

A final refinement of the analysis flow is shown in Figure 1(c) where now, the running sum technique could be integrated directly into the FEA analysis code. This would be a simple extension of existing routines that would allow the determination of the additional spectral moments needed to determine wideband response statistics.

3 Examples

Two different examples are presented below to show the use of the proposed running sum technique for determining response statistics. The first example is a simple cantilever beam, while the second is a complex telescope design whose response statistics can be efficiently determined by the proposed technique.

3.1 Cantilever beam

To illustrate the proposed computation technique, a cantilever beam example was developed. The beam has a constant cross section with length = 250 mm, width = 30 mm, height = 8 mm and was modeled with 10 uniform beam elements. The material was aluminum with elastic modulus $E = 69 \text{ N/m}^2$, Poisson ratio = 0.3 and mass density = $2800. \text{ kg/m}^3$. A uniform acceleration load of 1 g (9.81 m/s^2) was applied to develop unit modal forces. Table 1 gives the modal parameters for the first two bending modes of this model.

Mode	Eigenvalue λ (rad/s)	Eigenvector ϕ at end of beam	Modal Stress ξ at base of beam	Assumed Modal Damping δ	Modal Force γ
1	641.9	0.015371	-2.3794E + 06	0.005	-99,368
2	3978.5	0.015008	14.6667E + 06	0.005	55,210

Table 1: Modal parameters for cantilever beam example

A base excitation random acceleration load of $0.0002 \text{ g}^2/\text{Hz}$, from 10 to 800 Hz, was applied to the beam. Figure 2 shows the response tip displacement and base stress PSD curves for this analysis. A summary of the example results is given in Table 2.

Simulations at different frequency spacings Δf were run to study the stability of the response spectral moment estimates. The relative error RE in each of the response statistics was computed at each frequency spacing Δf_i as

$$RE(y)_i = \frac{y_i - y_{i-1}}{y_i} \quad (52)$$

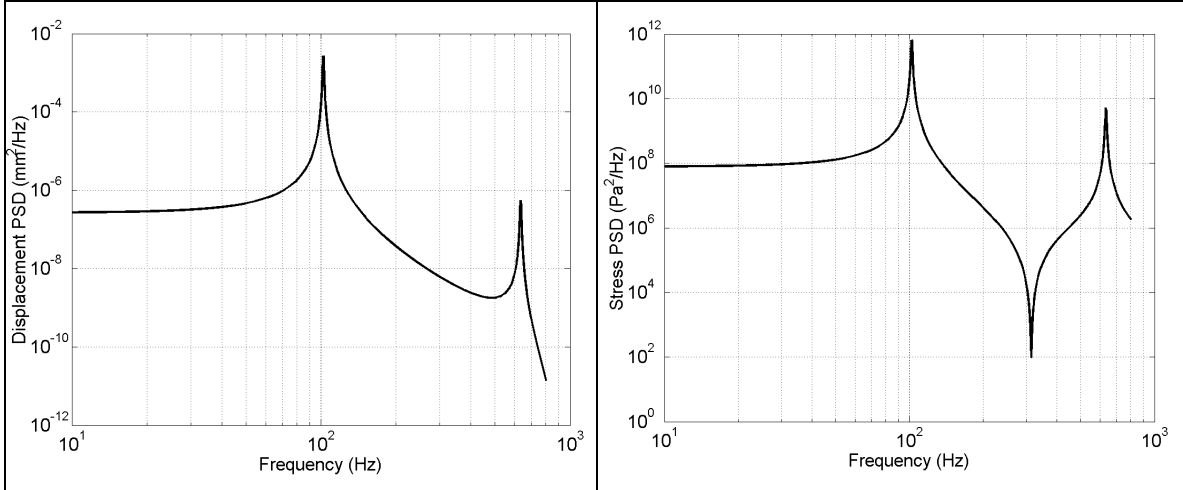


Figure 2: Response displacement and stress PSD for cantilever beam example

The half power bandwidth (*HPB*) of the first mode

$$\begin{aligned}
 HPB(\omega_i) &= 2\delta\lambda_i; \quad HPB(f_i) = \delta\lambda_i/\pi \\
 HPB(f_1) &= 0.005 * 641.9/\pi = 1.022 \text{ Hz}
 \end{aligned}
 \tag{53}$$

was used as to normalize the frequency spacing Δf to develop the plots shown in Figure 3 for both the displacement and the stress response statistics. The normalized x axis give an indication of the number of points across the *HPB* required for the rectangular integration to reach a certain relative error. The plots show that for this cantilever beam example, the relative error in all of the response statistics are below 10^{-3} given 3 points across the *HPB*. The plots also show that the relative errors level off at $\sim 10^{-6}$ given 5 points across the *HPB*.

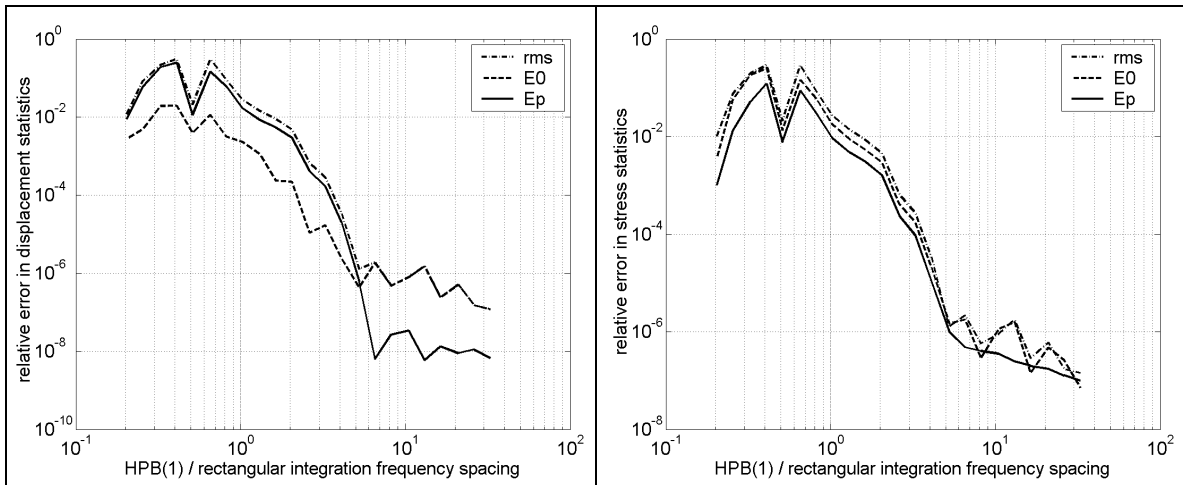


Figure 3: displacement and stress response statistics for different rectangular integration spacing

The positive peak displacement PDF, from (28) for this example, is shown in Figure 4(a). The displacement has been normalized by the rms value for convenient comparison to the limiting Rayleigh and Gaussian (normal) distribution PDFs. Notice that there are positive peaks that occur at negative displacements.

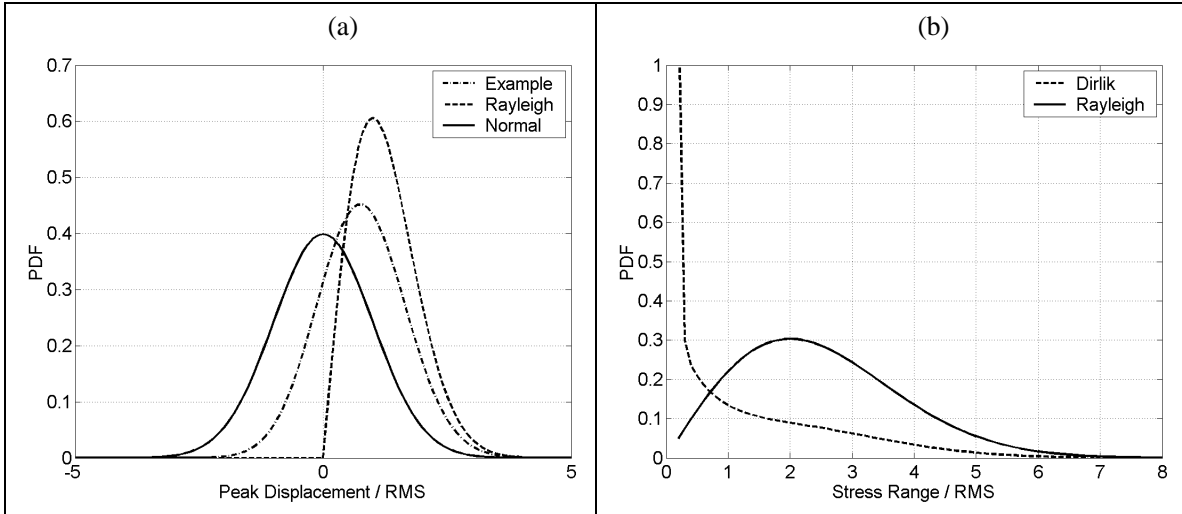


Figure 4: Normalized peak displacement and stress range PDFs for cantilever beam example

Insight into the fatigue life (and damage) estimates can be gained by plotting the stress range PDFs. Figure 4(b) is a normalized plot (i.e., stress range / rms stress) showing Rainflow range PDFs, labeled Dirlik (see (35)), compared to the Rayleigh PDF (see (31)). Notice the Dirlik estimate of the stress range PDF has a very different shape than the Rayleigh PDF. A “scaled damage PDF” [6] is shown over the normalized stress range for a fatigue exponent $\beta = 10$ in Figure 5(a). Figure 5(b) shows the cumulative result of (33) and (34) for a time T of 1 s and a material strength coefficient of $k = 10^8$. Note the scaled damage PDF has its median value at about 6.5X the rms for both theories, but the magnitude of the function based on narrow band theory (33) (labeled Rayleigh) is about 5X that of the wideband Dirlik theory (34). When these functions are integrated and multiplied by the expected rates ($E[0]$ for narrow band Rayleigh and $E[P]$ for wideband Dirlik), the results differ by only a factor of about 1.3.

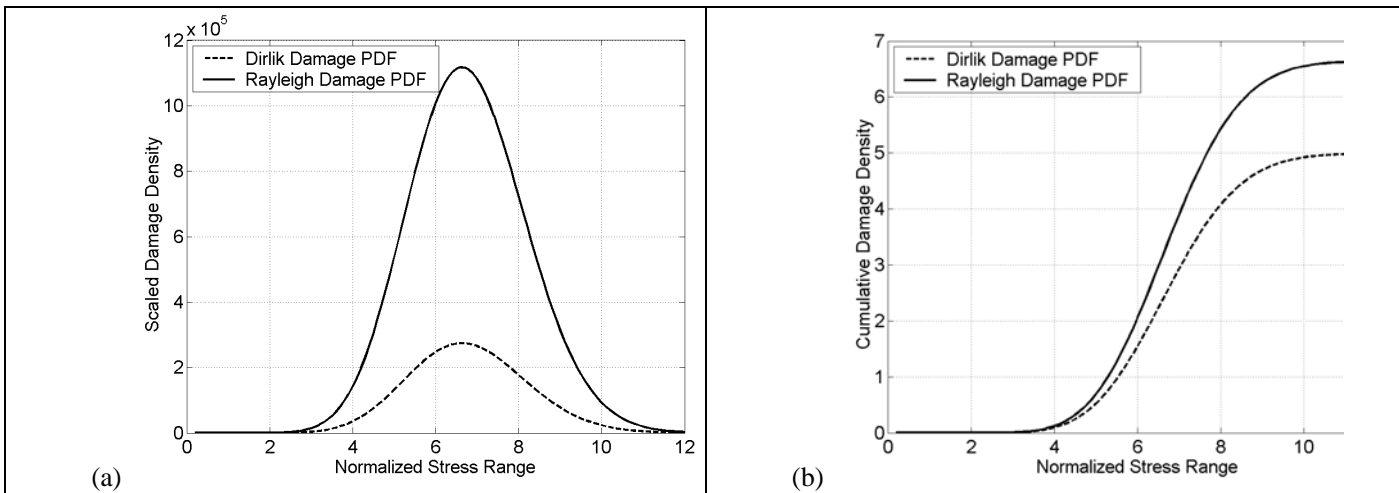


Figure 5: Scaled and cumulative damage densities with $\beta = 10$ for cantilever beam example

This cantilever beam example has shown how useful spectral moments can be for determining advanced-response statistics. The proposed running sum technique is a simple extension of mode superposition and can easily be implemented in analysis code. For this example, a standard analysis would have required ~25 kBytes of double-precision data to store the response PSDs for 1580 frequency points for 2 degrees of freedom. The 1580 points were the result of an analysis frequency spacing of 0.25 Hz (i.e., 4 points

across the *HPB*). The proposed running sum technique required ~ 80 Bytes to store the 5 modal parameters for 2 degrees of freedom. This is an improvement of over 300X in storage requirements.

Displacement Moments	Displacement Statistics	Stress Moments	Stress Statistics	Storage (Bytes)
M0 = 4.411E -03 M1 = 4.526E -01 M2 = 4.820E +01 M4 = 1.369E +06	rms = 0.0664 mm E[0] = 104.5 Hz E[P] = 168.5 Hz $\varpi = 0.6203$	M0 = 1.107E +12 M1 = 1.400E +14 M2 = 3.160E +16 M4 = 8.418E +21	rms = 1.052 MPa E[0] = 168.9 Hz E[P] = 516.2 Hz $\varpi = 0.3272$	Baseline = 25000 Running Sum = 80

Table 2: Cantilever beam example results summary

3.2 Earth-imaging optical telescope

The second example is based on an FEA model of an earth-imaging telescope. This model has two optical mirrored surfaces (primary (PM) and secondary (SM) mirrors) and an imaging detector as shown in Figure 6. This example model will be used to determine response statistics based on launch loads.

Although not presented here, on-orbit optical analysis can be simulated using modal Zernike coefficients, as outlined in section 1.4.3, with the proposed running sum technique [13].

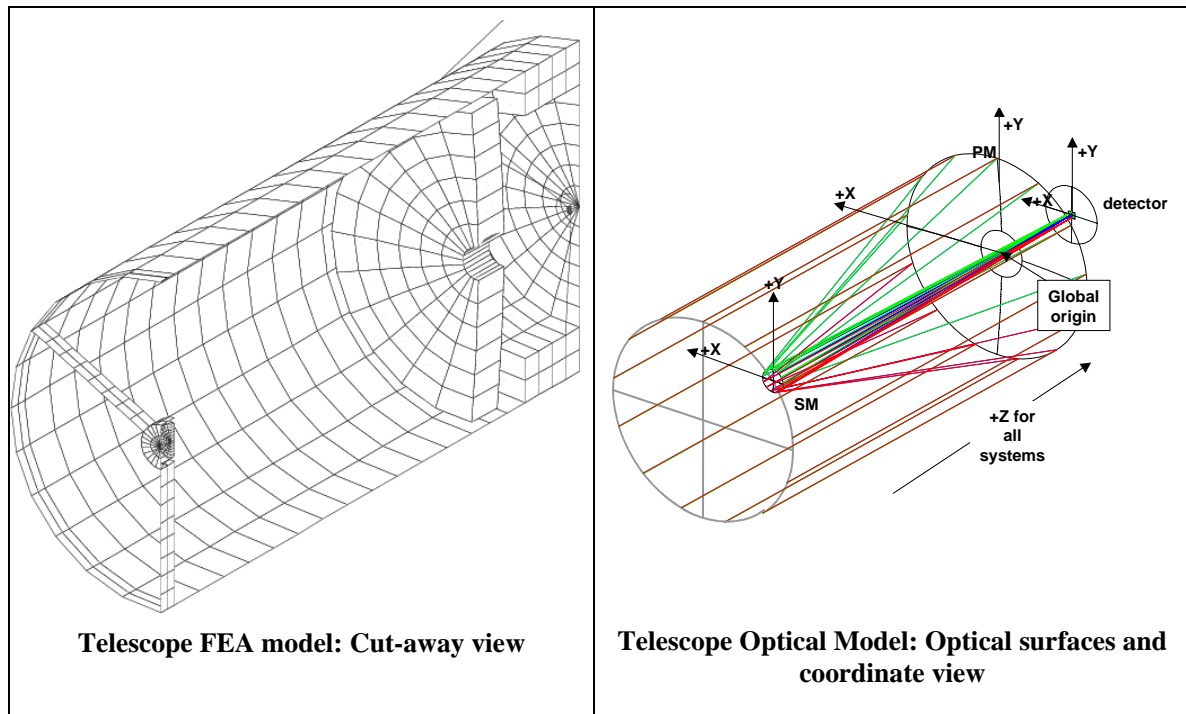


Figure 6: Earth-imaging telescope example model views

3.2.1 Launch load random input

One of the most challenging problems for an earth imaging payload is to design a light-weight telescope that is strong enough to withstand launch loads, while still being stable enough to operate on orbit. For this example, random vibration (see in Table 3) for 60 s, was input at the base of the telescope.

Frequency (Hz)	Acceleration PSD (g^2/Hz)
20	0.002
60	0.2
200	0.2
300	0.002

Table 3: Launch-load base random-vibration input (rms = 5.84 g)

3.2.2 Displacement response analysis

An important detail to verify in the telescope analysis is the clearance between the primary mirror (PM) and its surrounding structure. The radial displacement of the PM was analyzed in Nastran using multipoint constraint (MPC) equations to determine the difference between a set of response points. SigMax was used to perform the running-sum spectral-moment analysis. Table 4 gives a summary of the worst-case displacement point results from both simulations.

Program	rms Deflection	Spectral Moments	Response Rates	Peak Displacement
Nastran	0.4493 mm	NA	E[0] = 142.4 Hz	$P_N = 1.8153$ mm
SigMax	0.4493 mm	M0 = 2.019E -01 M1 = 2.634E +01 M2 = 4.092E +03 M4 = 1.346E +08	E[0] = 142.4 Hz E[P] = 181.4 Hz $\varpi = 0.7849$	$P_W = 1.8153$ mm

Table 4: Launch load relative displacement response results comparison

Peak displacement estimates based on a narrowband Rayleigh model with a zero crossing rate (Nastran results) and a wideband model with a peak rate (SigMax results), are given in the last column using the required 60 s of launch duration. The results are the same (to 10 significant digits) and show that, for this example, a narrow band approximation is adequate to describe the peak displacement. Plots of the peak PDF and the expected number of peak occurrences are given in Figure 7.

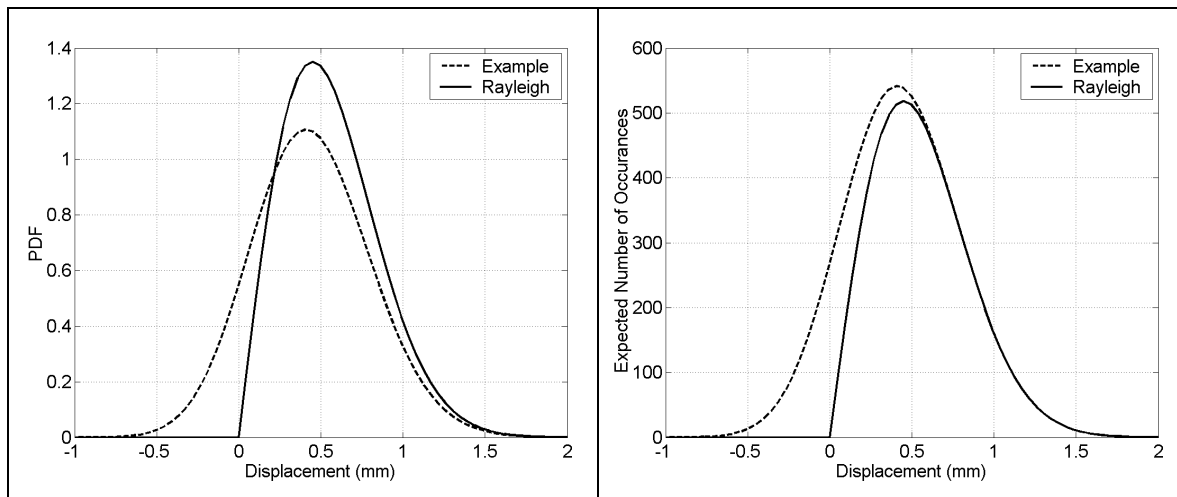


Figure 7: Peak mirror displacement and expected number of occurrences for telescope example

3.2.3 Stress response analysis

One of the most critical parts of a telescope design is that of the mirror mounts that need to be axially stiff, yet laterally flexible. This helps the structure stay in optical alignment, yet not be adversely influenced by other mechanical loads (e.g., thermal deformations). A fatigue analysis of the mirror mounts is a critical part of the verification process. A standard FEA Nastran analysis was run to produce random stress PSD response functions and estimates of the number of zero crossings. A running-sum spectral-moment analysis was also run in Sigmax. The results, at the most highly stressed element for both simulations, are given in Table 5.

Program	rms Stress	Spectral Moments	Response Rates	Damage
Nastran	38.48 Mpa	NA	E[0] = 191 Hz	E[D _N] = 2.471E -10
SigMax	38.48 Mpa	M0 = 1.478E +03 M1 = 2.789E +05 M2 = 5.391E +07 M4 = 2.138E +12	E[0] = 191 Hz E[P] = 199 Hz $\varpi = 0.9589$	E[D _w] = 2.353E -10

Table 5: Launch load stress response and damage results comparison

Damage estimates, based on a narrowband Rayleigh model (33) and a wideband Dirlik model (34), are given in the last column, assuming a Super Invar material [18] ($\beta = -1/b = 7.692$ and $k = 0.5*(2*\sigma_f)^b = 1.1354E + 27$). The results are very similar (which is due to the narrowband nature of the stress response, i.e., $\varpi \sim 1$) and show very low risk of fatigue damage. Plots of the stress range PDFs and cumulative damage are shown in Figure 8.

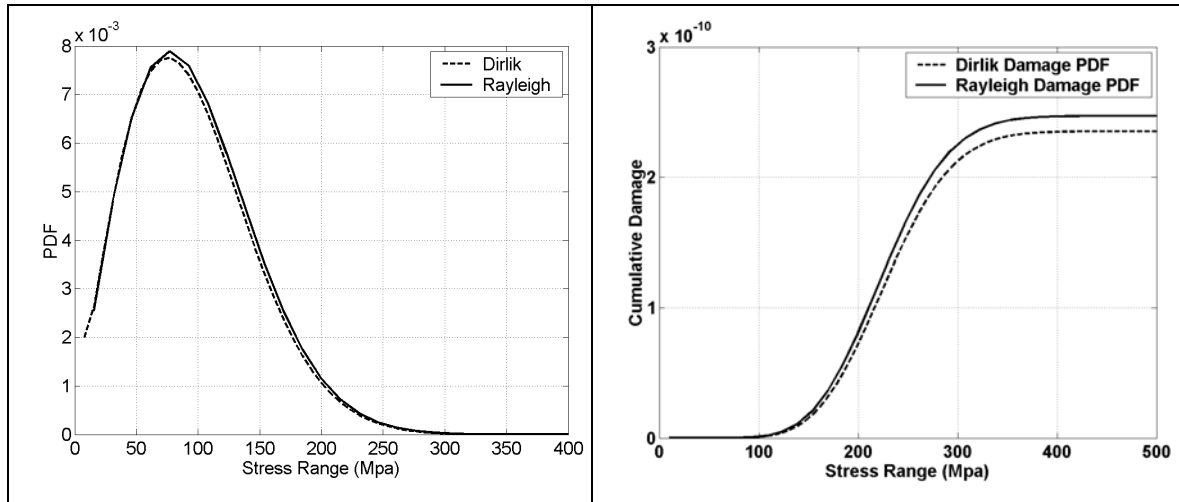


Figure 8: Stress range PDF and cumulative damage for primary mirror mount

For this telescope example, a standard analysis would have required ~98 MBytes of double-precision data to store the response PSDs for 1120 frequency points for 11,000 degrees of freedom. The proposed running sum technique required ~5.3 MBytes to store the 60 modal parameters for 11,000 degrees of freedom. This is an improvement of over 18X in storage requirements.

4 Conclusions

The concept of spectral moments has been presented. A new technique has been proposed for calculating these moments, which utilizes a running sum procedure. Examples show the utility of such an analysis procedure for determining peak displacement and stress statistics. The running sum technique can be easily extended to other linear modal transformations and higher order numerical integration methods.

Acknowledgements

The primary author thanks Eastman Kodak Company for their educational support at the ISVR.

References

- [1] J.S. Bendat, A.G. Piersol, *Random Data: Analysis and Measurement Procedures* (3rd edition), John Wiley (2000), pp. 170-186.
- [2] S.H. Crandall, C.H. Mark, *Random Vibrations in Mechanical Systems*, Academic Press (1963), pp. 44-53 & 103-125.
- [3] Y.K. Lin, *Probabilistic Theory of Structural Dynamics*, McGraw-Hill (1967), pp. 293-337.
- [4] D.E. Newland, *An Introduction to Random Vibrations and Spectral Analysis* (2nd edition), Longman Inc. (1984), pp. 82-94 & 189-196.
- [5] J. Miles, *On Structural Fatigue Under Random Loading*, Journal of Aeronautic Science, 21, (1954) pp. 753-762.
- [6] R.G. Lambert, *Analysis of Fatigue Under Random Vibration*, in *The Shock and Vibration Bulletin* No 46, Naval Research Laboratory, Washington, DC, (May 1976), pp. 55-72.
- [7] T. Dirlik, *Application of Computers in Fatigue Analysis*, University of Warwick Thesis, (1985).
- [8] N.W.M. Bishop, Sherratt, *Fatigue life prediction from power spectral density data. Part 1, traditional approaches and Part 2, recent developments*, Environmental Engineering, Vol. 2, No 1 and 2, (1989).
- [9] N.W.M. Bishop, F. Sherratt, *A theoretical solution for the estimation of rainflow ranges from power spectral density data*, Journal of Fatigue and Fracture of Engineering Materials in Structures, Vol. 13, (1990), pp. 311-326.
- [10] N.W.M. Bishop, *Dynamic fatigue response of deepwater offshore structures subjected to random loading*, Structural Engineering Review, 76/11, (1991), pp. 63-78.
- [11] D.J. Ewins, *Modal Testing: Theory and Practice*, Research Studies Press LTD. (1984) pp. 19-60.
- [12] K.A. Sweitzer, *Vibration Models Developed for Subsystem Test*, Syracuse University Masters Thesis, (1994), pp. 8-30.
- [13] V.L. Genberg, K.B. Doyle, G.J. Michels, *Optical Performance as a Function of Dynamic Mechanical Loading*, SPIE Paper 5178-4, (2003).
- [14] V.L. Genberg, *Optical Surface Evaluation*, SPIE Paper 450-508, (1983).
- [15] V.L. Genberg, G.J. Michels, K.B. Doyle, *Orthogonality of Zernike Polynomials*, SPIE Paper 4771-4833, (2002).
- [16] V.L. Genberg, *SigFit Reference Manual*, Sigmadyne, Inc., Rochester, NY, (2003).
- [17] V.L. Genberg, *Sigmax Software Documentation*, Sigmadyne, Inc., Rochester, NY, (1999).
- [18] A. Vinogradov, S. Hashimoto, V.I. Kopylov, *Enhanced strength and fatigue life of ultra-fine grain Fe/36Ni Invar alloy*, Materials Science and Engineering, A355, (2003), pp 277-285.